Published in final edited form as:
Eur J Neurosci. 2013 May ; 37(10): 1714–1725. doi:10.1111/ejn.12159.

γ-Secretase binding sites in aged and Alzheimer's disease human cerebrum: The choroid plexus as a putative origin of CSF Aβ

Fei Liu[1], **Zhi-Qin Xue**[2,3], **Si-Hao Deng**[2], **Xiong Kun**[2], **Xue-Gang Luo**[2], **Peter R. Patrylo**[4], **Gregory M. Rose**[4], **Huaibin Cai**[5], **Robert G. Struble**[4], **Yan Cai**[2], and **Xiao-Xin Yan**[2,*]

[1]Department of Neurosurgery, The Third Xiangya Hospital, Central South University, Changsha, Hunan 410013, China

[2]Department of Anatomy and Neurobiology, Central South University Xiangya School of Medicine, Changsha, Hunan 410013, China

[3]Department of Anatomy, Xinjiang Medical University, Urumqi, Xinjiang 830011, China

[4]Center for Integrated Research in Cognitive and Neural Sciences, Southern Illinois University Carbondale, IL 62901, USA

[5]Laboratory of Neurogenetics, National Institute on Aging, National Institutes of Health, Bethesda, MD 20892, USA

Abstract

Deposition of β-amyloid (Aβ) peptides, cleavage products of β-amyloid precursor protein (APP) by β-secretase-1 (BACE1) and γ-secretase, is a neuropathological hallmark of Alzheimer's disease (AD). γ-Secretase inhibition is a therapeutical anti-Aβ approach, although less is clear about the change of the enzyme's activity in AD brain. Cerebrospinal fluid (CSF) Aβ peptides are considered to derive from brain parenchyma, thus may serve as biomarkers for assessing cerebral amyloidosis and anti-Aβ efficacy. The present study compared active γ-secretase binding sites with Aβ deposition in aged and AD human cerebrum, and explored a possibility of Aβ production and secretion by the choroid plexus (CP). Specific binding density of [^{3}H]-L-685,458, a radiolabeled high affinity γ-secretase inhibitor, in the temporal neocortex and hippocampal formation was similar for AD and control cases with comparable ages and postmortem delays. The CP in postmortem samples exhibited exceptionally high [^{3}H]-L-685,458 binding density, with the estimated maximal binding sites (Bmax) reduced in the AD relative to control groups. Surgically resected human CP exhibited APP, BACE1 and presenilin-1 immunoreactivity, and β-site APP cleavage enzymatic activity. In primary culture, human CP cells also expressed these amyloidogenic proteins but released Aβ40 and Aβ42 into the medium. These results suggest that γ-secretase activity appears not altered in the cerebrum in AD related to aged control, nor correlated with regional amyloid plaque pathology. The choroid plexus appears to represent a novel non-neuronal source in the brain that may contribute Aβ into cerebrospinal fluid, probably at reduced levels in AD.

Keywords

β-amyloid; BACE1; γ-secretase; anti-Aβ therapy; AD biomarker

*Correspondence should be addressed to: Department of Anatomy and Neurobiology Central South University Xiangya School of Medicine Changsha, Hunan 410013, China Tel: 86-731-82650421 yanxiaoxin@csu.edu.cn.

Introduction

Deposition of β-amyloid (AƎ) peptides in the brain is a principal neuropathology of Alzheimer's disease (AD) (Hardy and Allsop, 1991; Selkoe, 1994). Current translational AD research includes the development of anti- AƎ therapies to reduce the production and/or to accelerate the clearance of the peptides in the brain (Ozudogru and Lippa, 2012). Biomarkers that may reflect brain amyloid metabolism, including AƎ in the cerebrospinal fluid (CSF), are being explored as means to assess the status/progress of cerebral amyloid pathogenesis and to monitor the efficacy of anti- AƎ therapy (Blennow et al., 2010; Rosenmann, 2012).

AƎ production involves proteolyses of Ǝ-amyloid precursor protein (APP) by Ǝ-secretase-1 (BACE1) and γ-secretase. BACE1 messenger, protein and activity appear to be elevated in the brain during aging and in AD, suggesting a role of BACE1 upregulation in AƎ overproduction (Vassar et al., 2009). Functional γ-secretase is a complex consisted of N- and C-terminal fragments of presenilins (PS1 and PS2), nicastrin, Aph-1, Pen-2 and TMP21 (Thinakaran et al., 1996; Kimberly et al., 2003; Laudon et al., 2004; Kaether, et al., 2006). Previous studies show variable results regarding the cellular/subcellular localization and abundance in the expression of PS1 and PS2 messengers, holoproteins or their N- and C-terminal fragments in familial and sporadic AD relative to control (Busciglio et al., 1997; Huynh et al., 1997; Levey et al., 1997; Chui et al., 1998; Weggen et al., 1998; Xia et al., 1998; Tomidokoro et al., 1999; Mathews et al., 2000; Panegyres and Toufexis, 2005). Recent studies suggest γ-secretase dysfunction in familial and sporadic AD (Hata et al., 2011, 2012; Chau et al., 2012; Chávez-Gutiérrez et al., 2012; Kakuda et al., 2012). Given its multimeric nature, conventional methods measuring γ-secretase subunit components may not necessarily reflect its functional status in vivo.

Many γ-secretase inhibitors have been developed and are under preclinical and clinical evaluations for therapeutic utility (Imbimbo and Giardina, 2011; Wolfe et al., 2012). Radiolabeled or biotinylated compounds, including compound D and L-685,458, have been also used as molecular probes for mapping active γ-secretase sites and activity in vitro and in vivo (Li et at., 2000, Yan et al., 2004; Patel et al., 2006; Goldstein et al., 2007; Xiong et al., 2007a; Frykman et al., 2010). In a previous study, γ-secretase binding sites assayed with [^{3}H]-compound D were found comparable in the cerebral cortex in a small group of AD relative to control cases (Patel et al., 2006). Given its clear pharmacological implications (Panza et al., 2010; Imbimbo and Giardina, 2011), we further explore the distribution and activity of γ-secretase related to amyloid pathology in a larger sample pool of AD and control cases, using [^{3}H]-L-685,458 as the radiotracer. While CSF AƎ levels are generally considered to be derived from the brain (Spies et al., 2012), it is of biological and clinical relevance to determine if there exist additional cellular contributors, especially the choroid plexus (CP) (Yan et al., 2004; Patel et al., 2006). We therefore explored the later possibility in the present study in vivo and in vitro.

Materials and methods

Brain sample and histological preparation

The use of postmortem and resected human brain samples and the experimental rats was in compliance with the Code of Ethics of the World Medical Association (Declaration of Helsinki) and the National Institute of Health Guide for the Care and Use of Laboratory Animals. Consent agreements were obtained from patients prior to neurosurgery for the collection and examination of brain biopsy. The experimental procedures in the present study were approved by the Animal Care and Use Committee of Southern Illinois University

at Carbondale and by the Research Ethics Committee at Central South University Xiangya School of Medicine.

Frozen temporal lobe slices (1–3 cm thick) from individuals without a history of dementia (Control group) and from clinically diagnosed AD patients or subjects with a history of dementia (defined as the AD group together) were obtained from the Analytical Biological Service (ABS) Inc. (Wilmington, DE, USA) and the AD Center of Southern Illinois University (SIU) (Table-1). Postmortem delay ranged from 3.5 to 38.5 hrs among these cases (P=0.767 between the means of the control and AD groups, two-tail paired Student's t-test). All AD cases from the SIU facility were diagnosed pathologically, with some cases also showed cerebral amyloid angiopathy (CAA) (Table-1). Neocortical and choroid plexus (CP) biopsies (n=5) were obtained at the Third Xiangya Hospital from patients suffered from intracerebral tumors (Table-1). The cortical samples (0.1-0.5 g) were resected from normal-appearing areas superficial or peripheral to the tumor in the temporal or parietal lobes. The CP samples (0.01-0.1 g) were resected while removing the tumor lesion involving the lateral ventricle. The biopsies were snap-frozen in liquid nitrogen then stored at −70 °C until use, or collected directly into a culture medium on ice for primary CP cell culture (detailed later).

Twenty adult male Sprague-Dawley rats were used to explore the effect of delayed tissue freezing (to mimic postmortem delay) on radioligand binding. The brains of 4 animals were removed and frozen immediately in liquid nitrogen after decapitation, then transferred into a −70 °C freezer. For the remaining animals, the brains were taken out 6, 12, 24 and 48 hrs (n=4 per time point) later after decapitation, during which the bodies were maintained at 4 °C.

Human and rat brain materials were cut at the frontal plane into equally-spaced (~500 :m) sets of sections at 20 :m (20 sets/brain) and 6 :m (12 sets/brain) thickness using a cryostat. Sections were thaw-mounted on positively charged Superfrost Plus slides (VWR, West Chester, PA, USA). A part of frozen CP samples were prepared into 6 :m sections mounted on slides. Cortical and CP biopsies were also used for biochemical studies. All frozen sections were properly labeled and re-stored at −70 °C until autoradiography and histological processing.

Primary human choroid plexus cell culture

Under sterile conditions, resected CP samples from 3 human subjects (CSU3-5, Table-1) were immediately collected into Dulbecco's Modified Eagle's Medium/Nutrient Mixture F12 (DMEM/F12, Life Technologies Corporation, Shanghai, China) on ice and transported to laboratory. The tissue was digested in 0.25% Trypsin-EDTA solution (Gbico 25200-072, Life Technologies Corporation, Shanghai, China), and centrifuged at 1200 rpm for 10 minutes. Cell pellets were re-suspended with DMEM/F12 containing 10% fetal bovine serum. The initial cell density in culture medium was adjusted to be approximately 5×10^6 cells/ml. CP primary culture was carried out in duplicate at 37°C in a humidified atmosphere containing 95% air and 5% CO_2, in 6-well Corning-Costar® plates (cat#CLS3516, Life Technologies Corporation, Shanghai, China). Each well was loaded with 2 ml of medium and a glass coverslip coated with polylysine. Phase contract images of cells were taken at 2, 4 and 8 days in dish (DID), with 200 :l of medium removed from each well at each time point (for A∃ assay) and re-supplied with the same volume of fresh medium. Finally, cells on coverslips were fixed on 8 DID in 4% paraformaldehyde for 30 minutes for immunocytochemistry.

Radio-labeled and cold γ-secretase inhibitors

The radioligand [^{3}H]-L-685,458 (0.5 mg in 0.5 ml 100% alcohol) was custom-tritiumized (Vitrax, Inc., Placenta, CA, USA) and purified by high-performance liquid chromatography (Xiong et al., 2007a). Specific activity of the final radioactive product was 10 ± 2 Ci/mmol, with a radiochemical purity >99%. Non-radioactive compounds included L-685,458 and its biotinylated derivatives L-852,505 and L-852,646 (Li et al., 2000; Xiong et al., 2007a), and a small molecule inhibitor, compound E (sc-222308, Santa Cruz biotechnology, Inc., CA, USA).

Autoradiography

In vitro autoradiography was batch-processed in duplicate for human and rat brain sections. Section-mounted slides were warmed from −70 °C to room temperature, preincubated in the HEPES assay buffer (50 mM HEPES, 10 mM $MgCl_2$, 2 mM EGTA, and 1 μg/ml each of aprotonin, leupeptin, and pepstatin), pH 7.2 at 23°C, for 10 min, then transferred into the same buffer containing 5 nM [^{3}H]-L-685,458 for 1 hr at room temperature. Another set of sections was processed in the presence of excessive cold ligands (0.5 uM) to define the nonspecific binding. L-685,458, L-852,505 and L-852,646 and compound E were tested as cold ligands in pilot studies, and they all blocked the specific binding to minimal nonspecific levels. Following the incubation with the hot ligand, sections were briefly washed twice (3 minutes each) with ice-cold phosphate buffered saline (PBS, 0.01M, pH7.4), dipped once in ice-cold distilled water, and dried against a stream of cold air. Saturation binding assay was conducted in sections containing the hippocampal formation to assess the maximal binding density (Bmax) and the dissociation constant (KD) in representative temporal lobe regions. Thus, seven adjacent sections were processed in parallel with gradient concentrations (0.1, 0.3, 1, 3, 10, 30, 100 nM) of the hot ligand only, together with an additional section processed with 100 nM hot ligand together with L-852,631 at 0.5 uM (to define non-specific binding). After autoradiographic binding, air-dried sections, together with [^{3}H]-microscales (GE Healthcare, USA), were placed under tritium-sensitive phosphor screens in darkness for 7 days.

Immunohistochemistry

Sections underwent autoradiography were immunolabeled for extracellular AƎ to correlate γ-secretase binding sites and amyloid pathology. Verification of AD pathologies (AƎ, p-tau and silver stain) and Nissl stain were carried out in other sections from all postmortem brains. Double immunofluorescence was conducted on 6 :m sections of the postmortem cortical and biopsied CP samples. Tissue fixation was done by immersion of the sections in 4% paraformaldehyde for 30 minutes, followed by 3 rinses in saline.

For immunohistochemistry with the peroxidase-DAB method, sections were treated with 1% H_2O_2 in PBS for 30 minutes, and pre-incubated in 5% normal horse serum with 0.1% Triton X-100 for 1 hr. For BACE1 and AƎ antibody staining, sections were else pretreated in 50% formamide and 50% 2XSSC (0.15 M sodium chloride and 0.015 M sodium citrate) at 65 °C for 30 minutes and 50% formic acid at room temperature for 30 minutes, respectively. Sections were then incubated overnight at 4 °C with primary antibodies in PBS, including (1) mouse anti- AƎ1-16, 6E10 (Signet, USA, #39320, 1:4000); (2) rabbit anti-BACE1 (against amino acid residues 46-163 of human BACE1, 1:2000) (Xiong et al., 2007b; Zhang et al., 2009); (3) rabbit anti-phosphorylated-tau (p-Ser199/Ser202) (Sigma-Aldrich, T6819, 1:3000) (Cai et al., 2012). The sections were next reacted with a biotinylated pan-specific secondary antibody (horse anti-mouse, rabbit and goat IgG) at 1:400 for 1 hr, and then in avidin-biotin complex (ABC) solution (1:400) (Vector Laboratories, Burlingame, CA, USA) for an additional hr. Final immunoreactivity product was visualized in 0.003% H_2O_2 and 0.05% diaminobenzidine (DAB). Sections were washed with PBS for 3 times, 10 minute

each, between incubations. To define the level of non-specific reactivity, several sections were processed with the above procedures except for the exposure to the primary antibodies.

Immunoflourescence (single or double labeling) was carried out on cryostat CP sections and CP cell coverslips, using a set of well-characterized antibodies to APP (22C11, 1:2000), and BACE1 (1:1000), presenilin-1 (rabbit anti-PS1 N-terminus, ab14, 1:1000, courtesy from Dr. S. Gandy) (Thinakaran et al., 1996), 6E10 (Signet, #39320, 1:2000); F-actin (Serotec, monoclonal mouse anti-human F-actin antibody, MCA358G, 1:2000) (Baehr et al., 2006), glucose transporter-1 (GLUT-1) (Millipore, USA, rabbit anti-GLUT-1, CBL242, 1:500) (Cornford et al., 1998), glial fibrillary acidic protein (GFAP) (Sigma-Aldrich, rabbit anti-GFAP, G9269, 1:2,000) and microtubule associated protein-2 (MAP2) (Sigma-Aldrich, mouse anti-MAP2, M9942, 1:2,000). Sections were first incubated in PBS containing one or a pair (from mouse and rabbit) of primary antibodies and 5% donkey serum, followed by a 2 hr reaction with Alexa Fluor® 488 and Fluor® 594 conjugated donkey antibodies against mouse or rabbit IgGs (1:200, Invitrogen, Carlsbad, CA, USA). The sections were then dipped in PBS containing bisbenzimide (Hoechst 33342, 1:50000), washed and mounted with anti-fading medium.

Western blot

Cortical and CP biopsies were homogenized in T-PER buffer (10x w/v) (Pierce, Rockford, IL, USA) containing protease inhibitors, and centrifuged at 15,000 X g at 4 °C for 10 minutes. The supernatants were collected and subjected to DC protein assay (Bio-Rad Laboratories, Hercules, CA, USA). Samples containing 25 μg of protein were loaded in 4-20% SDS-PAGE gradient gel (Bio-Rad Laboratories), with separated polypeptides electrotransferred to Trans-Blot® pure nitrocellulose membrane immunoblotted for BACE1 (1:1000), APP (22C11, 1:4000), APP Ǝ-site cleavage products C89 and C99 (6E10, 1:2000) and glyceraldehyde-3-phosphate dehydrogenase (GAPDH, Millipore, MAB374, 1:5000). Immunoblot products were visualized using HRP-conjugated goat anti-rabbit or anti-mouse IgG (1:20000, Bio-Rad Laboratories) and the ECL Plus™ Western Blotting Detection kit (GE Healthcare, Piscataway, NJ, USA), and imaged in a UVP Biodoc-itTM system (UVP, Inc., Upland, CA, USA).

Enzyme activity assay for Ǝ-site APP cleavage

Ǝ-Site APP cleavage activities in biopsied cortical and CP samples (homogenized as above) were measured in 96-well transparent flat-bottomed plates. Samples were assayed using a commercial kit (Calbiochem, La Jolla, CA, USA, #565785), following the manufacturer's instructions. The fluorescent signal was captured in a Bio-Rad microplate reader (PR 3100 TSC), with the data normalized to the mean of the cortical samples for statistical comparison.

ELISA for Aβ in culture medium

Media (50 :l/well) from human CP primary cultures were assayed in duplicate by enzyme-linked immunosorbnent assay (ELISA) to assess AƎ40 and AƎ42 levels, using commercial kits (Novex® KHB3482 for AƎ40 and KHB3442 for AƎ42) following the manufacturer's instruction (Life Technologies Corporation, Shanghai, China). The signals were captured in the Bio-Rad plate-reader, with synthesized peptides at tittered concentrations assayed concurrently for calibration. AƎ levels (pg/ml) were obtained from 2 culture wells in each case (n=3) to estimate the amount of secreted peptides following cultivation for 2, 4 and 8 days.

Imaging and data analysis

Autoradiographic images were captured with a Cyclone phosphor imaging scanner controlled by the OptiQuant acquisition and analysis software (Parkard Instruments, Meriden, CT). Optic densities (expressed as digital light units per square millimeter, DLU/mm^2) over areas of interest (grey matter over the superior and middle temporal gyri or individual hippocampal layers) and the [^{3}H] standards were measured. Specific optic density was calculated by subtracting nonspecific binding signal from total binding at the same region. Means were calculated and converted to femtomoles per milligram (fmol/mg) of tissue equivalent, when appropriate, according to a curve generated from readings over ^{3}H standards and the specific radioactivity of the radioligand. Densitometry for amyloid pathology (6E10) in the same sections subjected to autoradiography was carried out using a threshold selection approach. Thus, optic densities of 6E10 reactivity over the same areas quantified for radioligand binding were measured with the OptiQuant software. Non-specific signal from sections processed in the absence of 6E10 incubation was also obtained, which was used as the cutoff for calculating specific optic densities of the amyloid plaques. The autographic and immunohistological quantifications were analyzed by two different experimenters who were blinded to case information. To estimate the density of cultured human CP cells (at 8 DID), images of bisbenzimide-stained nuclei were captured using 4X objective across the coverslip, followed by image montage. The number of stained cells on, and the area of, the coverslip were measured, yielding densitometric figures. For western blot images, optic densities of target protein bands were standardized to the levels of GAPDH in corresponding samples (expressed as % GAPDH optic density).

All optic density readings were input into Excel spreadsheets. Mean [^{3}H]-L-685,458 binding and 6E10 labeling densities in the temporal neocortex of each case were calculated based on measurements from 4 equally-spaced (~500 :m) sections. Saturation binding data were processed with the Prism (Prism GraphPad, San Diego, CA, USA) software using one-site binding mode (hyperbola) to estimate the Bmax and KD. Means were compared statistically with ANOVA, Student's *t*-test or correlation analysis. The minimal significant level of difference was set at $P < 0.05$. Figure panels were assembled with CorelDRAW 10 and Photoshop 7.1.

Results

Pathological evaluation of postmortem brain samples

The definitive diagnosis of some AD cases in the present study (those from SIU AD center) was established by standard postmortem pathological evaluation (Struble et al., 2010). We checked AD-like neuropathology in all human brain samples using Bielschowsky stain and immunolabeling for AƎ and p-tau. Amyloid plaques and neurofibrillary tangles were found in the temporal cortex and hippocampal formation in all AD cases, whereas most control cases exhibited neither lesion. Cerebral amyloid pathology also existed in about 1/4 of the non-AD cases, generally to a lesser extent as compared to the AD group (see quantitative data later). Increased BACE1 immunoreactivity (IR) in dystrophic neurites was detectable arround some compact-like amyloid plaques (data not shown, but see Cai et al., 2010, 2012).

Effect of delayed tissue freezing on [^{3}H]-L-685,458 binding

In a pilot study with a small group of cases we noticed considerable individual variability in [^{3}H]-L-685,458 binding density in the cortex. This raised our concern that postmortem delay might affect radioligand binding, thus limiting the application of autoradiography in assessing γ-secretase binding sites in postmortem human brain. One way to resolve this issue would be to increase the sample size. However, we considered it also important to evaluate the extent to which postmortem delay might influence [^{3}H]-L-685,458 binding

density in the brain. The latter attempt was experimentally assessed by comparing binding densities in the cerebral cortex of the adult rats with their brains removed/frozen immediately and following different periods of "postmortem" delay after decapitation. Identical histological and autoradiographic procedures were applied to all rat brain samples using a batch-processing approach.

Compared to fresh frozen samples, a decline in [^{3}H]-L-685,458 binding density occurred in parallel in the cerebral cortical grey matter and the hippocampal formation with the increase of time delay of brain removal and freezing (Fig. 1A-E). Thus, specific binding density in the parietotemporal cortex reduced to 92.2±4.9%, 79.3±9.0%, 46.1±8.3% and 19.5±5.2% after 6, 12, 24 and 48 hrs of time delay (100 ±6.0%) ($P<0.0001$, $F=96.4$, df=4,15, one-way ANOVA analysis). Posthoc tests indicated that the reduction was significant at 24 hrs ($P<0.005$) and 48 hrs ($P<0.001$), but not at 12 hrs ($P>0.05$) (however, $P=0.039$ by one-tail paired student's *t*-test). The reductions in [^{3}H]-L-685,458 binding density in the hippocampal formation (including Ammon's horn and dentate gyrus) were closely similar to that in the cortex, i.e., 94.7±6.7%, 82.2±3.6%, 44.2±8.2% and 13.2±7.9% at 6, 12, 24 and 48 hrs, relative to 0 hr (100 ±6.2%), delay of brain freezing ($P<0.0001$, $F=121.7$, df=4,15), with the drop appeared approaching significance at 12 hrs ($P=0.076$ by one-tail paired student's *t*-test, $P>0.05$ by post-hoc), and statistically significant at 24 hrs ($P<0.0001$) and 48 hrs ($P<0.0001$) time points (Fig. 2F).

[^{3}H]-L-685,458 binding density relative to amyloid plaque abundance

To compare the densities of [^{3}H]-L-685,458 binding sites and extracellular AƎ deposition in the same cortical areas in individual AD and control cases, sections processed with autoradiography were immunostained with the 6E10 antibody (Fig. 2A-M). Thus, specific densities measured over the temporal cortical grey matter (layers I-VI) were plotted against individual cases and subjected group mean comparison. Postmortem delays were included in the correlative analysis. Between the control (n=14) and AD (n=14) groups, the means of postmortem delay were not significantly different ($P=0.626$, two-tail student-*t* test) (Fig. 2N). The mean specific densities of [^{3}H]-L-685,458 binding sites were comparable between the AD (53,061±10,287 DLU/mm^2) and control (58,894±10,245 DLU/mm^2) groups ($P=0.145$, paired two-tail student-*t* test, Fig. 2O). In contrast, the mean specific density of amyloid plaques in the AD group (19,814±8,071 DLU/mm^2) was significantly higher relative to the control group (3,255±3,544 DLU/mm^2) ($P<0.0001$, two-tail student-*t* test, Fig. 2P). Notably, [^{3}H]-L-685,458 binding density was particular lower in one control and one AD cases with postmortem delays longer than 10 hrs (Fig. 2E, K, N, and O). When these two cases were excluded from analysis, there was also no difference in [^{3}H]-L-685,458 binding density between the AD and control groups (data not shown). We carried out correlation analyses for [^{3}H]-L-685,458 binding density among cases with postmortem delays less than 10 hrs in the control, AD or both groups, which did no yield an apparent correlation between the two variables. Also, no correlation was found between amyloid density and postmortem delay among the cases in the control or AD group (data not shown).

Spatial relationship between [^{3}H]-L-685,458 binding sites and amyloid plaques

Besides the above correlative densitometry, we assessed if there existed a spatial relationship between [^{3}H]-L-685,458 binding sites and extracellular AƎ deposition. The hippocampal formation was used for this comparison because it exhibited apparently differential regional/laminar distribution of [^{3}H]-L-685,458 binding sites and amyloid plaques. Overall, there was no difference in laminar distribution of [^{3}H]-L-685,458 binding sites in AD and control hippocampal formation. Quantification was carried out to reveal a laminar difference in binding density using the AD (n=5) and control (n=5) cases with postmortem delay < 6 hrs. The hilus and CA3 exhibited the most abundant binding sites,

likely due to the heavy expression of γ-secretase complex in the mossy fiber terminals (Yan et al., 2004; Xiong et al., 2007a). Moderate binding sites occurred in CA1 stratum pyramidale, subicular cortex (layers II-III) and the dentate molecular layer (Fig. 3A, F). Examination of the autoradiographic and immunolabeling images from the same section indicated that there lacked a laminar or regional correlation between binding sites and Aβ deposition. Shown as an example from the AD group (Fig. 3A-D), the amyloid plaques were fairly abundant in the dentate molecular layer and the hippocampal strata lacunosum and radiatum, wherein [^{3}H]-L-685,458 binding density was actually considerably low without apparent uneven (or plaque-like) distribution by visual examination (Fig. 3A-D). Most distinctly, there were few amyloid plaques around the mossy fiber terminal area in the hilus and CA3, despite a dense presence of [^{3}H]-L-685,458 binding sites.

Expression of amyloidogenic proteins at the cerebral choroid plexus

[^{3}H]-L-685,458 binding sites were present at the CP of the lateral ventricle in both the control and AD human brains (Fig. 3A), consistent with the pattern seen in rodents and nonhuman primates (Fig. 1A, C) (Yan et al., 2004; Patel et al., 2006). Quantitatively, the binding density here exceeded that at the mossy fiber terminal areas (Fig. 3F). This prompted us to assess the Bmax and KD in the CP relative to some hippocampal lamina, with saturation binding assays using temporal lobe sections containing the CP from control (n=5) and AD (n=5) cases with postmortem delays ≤ 6 hrs (Fig. 3G). [^{3}H]-L-685,458 binding was saturable in various temporal lobe areas in the control or AD brain. The saturation curves were essentially overlapped in control and AD samples for binding sites in the subiculum and CA3 (mossy fiber terminal field), but appeared differential for that in the CP (Fig. 3F). Means of estimated Bmax values showed significant difference between the two groups for the CP (907.8±38.4 fmol/mg in control vs 840.4±39.3 fmol/mg in AD; P=0.0456, paired two-tail student's *t*-test), but not for the subiculum and CA3 regions. Estimated KD was comparable between the control and AD groups for the 3 analyzed areas (Fig. 3F, inserted table).

The exceptionally abundant γ-secretase expression in the CP might suggest a novel non-neuronal structure in the brain that secretes Aβ into the CSF. Thus, it was considered also important to determine whether the CP might express APP and BACE1. Biopsied human samples were used to explore this issue biochemically and immunohistochemically. We first verified the presence and specificity of BACE1 expression in the CP using brain sections from BACE1 knockout (BACE1−/−) mice and wild-type (BACE+/+) littermates (Zhang et al., 2009). As with neuronal components, BACE1 IR was absent in the CP in BACE1−/− brain, but present in BACE1+/+ counterpart (Fig. 4A-C). In double immunofluorescence, human CP cells co-expressed APP (22C11 IR) and BACE1 (Fig. 4D-F). These cells also exhibited colocalized 6E10 and BACE1 IR (not shown). As expected based on autographic γ-secretase binding data, resected human CP cells expressed immunolabeling for presenilin-1 (Fig. 4G, H). Of note, in postmortem tissue the intensity of 6E10 IR in the CP cells was apparently lower relative to extracellular plaque labeling, but appeared to be somewhat stronger relative to some faint neuronal perikaryal reactivity seen in some areas, including the CA sectors (Fig. 3B-E). Given that 6E10 can label human APP, the intracellular 6E10 IR seen in neuronal somata and the CP might, probably, largely relate to APP expression (Stern et al., 1989; Winton et al., 2011).

We also checked APP and BACE1 protein levels, and β-site cleavage enzymatic activity, in the biopsied CP relative to cortical extracts from the same group of adult human subjects. The levels of APP (P=0.013, paired two-tail student's *t*-test) and BACE1 (P=0.009, two-tail student's *t*-test) proteins were relatively higher in the CP than cortical homogenates (Fig. 4I, K). β-Site APP cleavage products, C99 and C89, were detectable in the CP homogenates

(Fig. 4J). ∃-Site cleavage activity in the CP extracts was nearly 2 fold of that in the cortical counterparts (defined as 100 %) ($P<0.001$, two-tail student's *t*-test) (Fig. 4L).

Secretion of A∃ peptides by primary human choroid plexus cells

Following 2 days of culture, a small amount of CP cells were seen under inverted phase contrast microscope (Fig. 5A). The cells covered approximately 10% surface area of the culture dish bottom or coversplip (by visual scoring). At 4 DID, the cells appeared to grow over ~50% surface area at the dish bottom (Fig. 5B), and by 8 DID, a monolayer of cells formed, occupying most surface area (80-100%) (Fig. 5C). CP cell densities were determined at 8 DID by quantifying bisbenzimide positive nuclei on the coverslips. The mean density of the labeled cells was 636.7±59.8 cells/mm^2 (579. 2 for case CSU3, 632.3 for CSU4, and 697.6 for CSU5) .

The cultured cells exhibited morphological and some biochemical features of human CP epithelial cells shown in previous studies. Thus, they were often in a polygonal shape at 2 and 4 DID (Fig. 5A, B) (Mestres-Ventura et al., 2012), and appeared mostly fusiform at 8 DID as the cells became closely packed (Fig. 5C). The cultured cells showed distinct cytoskeleton configuration in F-actin immunoflourescence (Fig. 5D) (Baehr et al., 2006), and expressed clear immunolabeling for GLUT-1 (Fig. 5E) (Cornford et al., 1998). As expected (Fig. 4E, F, H), these cultured CP cells were immunoreactive for APP (Fig. 5F), BACE1 (Fig. 5G) and PS1 (Fig. 5H). In contrast, the cells were not immunoreactive for the typical astrocytic marker GFAP or the neuronal marker MAP2 (data not shown).

At 2 DID, A∃40 (−0.92±1.72 pg/ml) and A∃42 (3.36±2.63 pg/ml) in the culture media were not detectable or very low (Fig. 5I). The A∃ concentrations were increased at the two later in vitro time points, especially dramatic for A∃42. Thus, the concentrations of A∃40 were 3.91±2.71 pg/ml and 65.33±21.85 pg/ml at 4 DID and 8 DID, respectively. A∃42 levels reached to 170.16±92.98 pg/ml at 4 DID and 461.35±123.58 pg/ml at 8 DID. Statistically (one-way ANOVA), there existed a time-dependent elevation for both A∃40 ($P=0.0004$, $F=36.30$, $df=2, 6$) and A∃42 ($P=0.0019$, $F=21.27$, $df=2, 6$) in the culture medium (Fig. 5I).

Discussion

γ-Secretase binding sites are not apparently altered in AD cerebral cortex

Hypothetically, a drug targeting an overactive pathogenic factor would be expected to offer the maximal pharmacological benefit for normalizing the corresponding excessive disease-causing products. In this regard, it is of clinical relevance to determine whether γ-secretase activity elevates in AD human brain. Because γ-secretase is a multimeric complex, molecular probes, such as specific enzyme inhibitors that highlight the anatomical/functional properties of the enzyme *in situ* are especially useful to address its biological, pathological and pharmacological implications *in vivo*. Assayed with [^{3}H]-compound D (Patel et al., 2006), γ-secretase binding in human brain homogenates exhibits high affinity to a single site, with the estimated Bmax or KD comparable between AD and control membranes (n = 3-5). [^{3}H]-compound D binding sites appear not to spatially correlate with amyloid plaques as assessed between adjacent sections.

In the present study we obtained cerebral samples from 14 control and 14 AD human brains, with postmortem delays and ages statistically comparable between the two groups. An analysis using adult rat brains harvested with post-decapitation delays suggests that γ-secretase binding sites reduce in the cerebral cortex and hippocampal formation largely after 12 hrs of delay. This finding is consistent with the observation in the human brain that [^{3}H]-L-685,458 binding sites appear to be well preserved in the cerebral cortex and hippocampal formation in the majority of cases (with postmortem < 10 hrs). In fact, the regional and

laminar distribution patterns of [^{3}H]-L-685,458 binding sites in various temporal lobe structures are essentially comparable or consistent with that seen in rodents and non-human primates (Yan et al., 2004; Patel et al., 2006; Xiong et al., 2007a). This information, together with the use of a sufficient sample size, led us conclude that the data from the current cohort would closely reflect the anatomical and functional conditions of γ-secretase complex in AD relative to non-AD human brains.

Quantitatively, the overall specific γ-secretase binding density measured in the temporal neocortex or the hippocampal formation (data not presented) is comparable between the control and AD groups. Our correlative densitometric analysis also indicates a lack of association between γ-secretase binding density and amyloid plaque abundance in the neocortex among individual subjects either in the control or the AD group. Further, there is no apparent change in regional and laminar distribution pattern of γ-secretase binding sites among the temporal lobe structures in AD relative to control brains. Finally, same-section anatomical analysis fails to find a spatial correlation between γ-secretase binding sites and plaque localization. Thus, the present study extends the previous finding that γ-secretase binding sites (Patel et al., 2006), hence the localization and activity of the enzyme complex, are probably not altered in the cerebral neocortex and hippocampal formation in AD relative to aged non-AD human subjects.

However, it is difficult to determine the extent to which the γ-secretase binding sites revealed by [^{3}H]-compound D or [^{3}H]-L-685,458 relates to the enzyme's amyloidogenic activity in vivo. This is because γ-secretase is involved in proteolytic processing of many other type-I membrane proteins than APP (Iwatsubo, 2004; Raemaekers et al., 2005; Kaether et al., 2006). For APP processing, γ-secretase is also a part of the non-amyloidogenic pathway, which is believed to be predominant (than the amyloidogenic processing) under physiological conditions. Thus, from a biological perspective, one may speculate that γ-secretase expression and activity might be redundant in the brain to ensure its multiple functions. As such, the overall, perhaps the APP processing or even amyloidogenic, γ-secretase activity may be not necessarily changed in AD or play a key role in determining the amyloidogenic vulnerability. The results of the present study appear to be suited with such reasoning. However, future studies, including clinical trials of target-specific (e.g., Notch-1 sparing) γ-secretase inhibitors in humans, will be needed for a definitive answer as to whether and to what extent γ-secretase alteration is involved in Aβ overproduction and plaque pathogenesis in AD, and whether pharmacological inhibition of this enzyme can indeed achieve the expected therapeutic efficacy.

The choroid plexus may contribute a certain amount of Aβ into cerebrospinal fluid

CSF Aβ has been explored as a biomarker for AD during the past 15 years (Engelborghs et al., 2007; Holtzman, 2011), with a growing interest in recent years in searching for a measure to monitor the effect of anti-Aβ therapies in clinic (Mattson et al., 2009; Parnetti and Chiasserini, 2011; Lu et al., 2012; Vanderstichele et al., 2012). Specifically, CSF Aβ42 levels are lowered in AD relative to control, and decline during the transition from predromal to definitive AD stages (Skoog et al., 2003; Buchhave et al., 2012). The lowering of CSF Aβ42 suggests reduced amyloid clearance from brain parenchyma, causing cerebral Aβ accumulation and plaque development (http://www.alzforum.org/res/adh/cur/knowntheamyloidcascade.asp). Notably, CSF Aβ42 levels are lowered in number of other neurological conditions than AD (Otto et al., 2000; Noguchi et al., 2005; Bibl et al., 2006; Kapaki et al., 2007; Siderowf et al., 2010; Mollenhauer et al., 2011; Koedam et al., 2012; Krut et al., 2012; Pomara et al., 2012). CSF Aβ42 concentration may vary as measured by different laboratories or using different protocols (Dumurgier et al., 2012). CSF Aβ levels in the same individuals may show variability when measured at different times (Slats et al., 2012). In human the CP may produce ~500 ml of CSF daily, counting for approximately 3.7

times of overall turnover in a single day (http://en.wikipedia.org/wiki/Cerebrospinal_fluid). Such a high turnover rate could alter (dilute) the concentration of CSF AƎ peptides derived from brain parenchyma, representing a factor that may cause variation of measured AƎ levels. Thus, CSF AƎ data should be evaluated by taking consideration of physiological or pathophysiological conditions that might cause or be associated with change in CSF dynamics (Redzic et al., 2005; Spies et al., 2012).

The CP has been suggested to transport but also produce AƎ (Kalaria et al., 1996; Sasaki et al., 1997). The strikingly high expression of γ-secretase binding sites in the CP implicates that this structure *per se* might produce/secrete significant amounts of AƎ directly into the CSF. The present study has further characterized that human CP cells express APP, BACE1 and PS1 proteins in vivo and in vitro, and exhibit a capability for enzymatic Ǝ-site APP cleavage. Importantly, cultured human CP cells also possess a full set of protein machinery for AƎ genesis, but appear to produce and secrete AƎ40 and AƎ42 into culture medium. While our biochemical data also suggest a higher Ǝ-site APP cleavage activity in the CP than cortical homogenates, additional studies are needed to determine whether CP cells are more capable of AƎ secretion than neural cells.

Human CP may undergo pathological changes and functional impairments during aging and in AD (Serot et al., 2000; Preston et al., 2001; Wolburg and Paulus, 2010; Krzyzanowska and Carro, 2012). Besides impaired transportation/clearance functions, the CP cells may produce less CSF with aging and during AD development (Silverberg et al., 2001; Serot et al., 2011). With this regard, the finding of a reduced Bmax of γ-secretase binding sites in the present study appears to warrant further investigation, to clarify if AƎ genesis by the CP is reduced and may account for, at least in part, the reduced CSF AƎ levels during aging or AD development. Meanwhile, a CP-related AƎ genesis should be probably taken into consideration while using CSF AƎ levels to monitor the effect of anti- AƎ therapies in clinical settings.

In summary, the present study shows that the overall density and distribution of γ-secretase binding sites are comparable in the temporal neocortex and hippocampal formation between AD and aged non-AD human subjects. There is also no obvious spatial correlation between cerebral γ-secretase binding sites and extracellular amyloid plaques. Human choroid plexus cells co-express the substrates and enzymes known for AƎ genesis, and secrete AƎ40 and AƎ42 peptides in vitro, suggesting a non-neuronal niche in the brain to contribute these peptides in the cerebrospinal fluid.

Acknowledgments

This study was supported by Southern Illinois University School of Medicine (CRC grant to X.X.Y.), National Natural Science Foundation of China (#81171091 to X.X.Y. and #81171160 to X.G.L.) and the intramural research program of National Institute on Aging, NIH (Z01-IAAG000944-04 to H.C.). We thank Dr. Robert Fazio at Vitrax, California for compound tritiumization, Dr. Yue-Ming Li for providing some cold γ-secretase inhibitors, and Dr. San Gandy for providing the PS1 antibody.

References

Baehr C, Reichel V, Fricker G. Choroid plexus epithelial monolayers-a cell culture model from porcine brain. Cerebrospinal Fluid Res. 2006; 3:13. [PubMed: 17184532]

Bibl M, Mollenhauer B, Esselmann H, Lewczuk P, Klafki HW, Sparbier K, Smirnov A, Cepek L, Trenkwalder C, Rüther E, Kornhuber J, Otto M, Wiltfang J. CSF amyloid-beta-peptides in Alzheimer's disease, dementia with Lewy bodies and Parkinson's disease dementia. Brain. 2006; 2129(Pt 5):1177–1187. [PubMed: 16600985]

Blennow K, Hampel H, Weiner M, Zetterberg H. Cerebrospinal fluid and plasma biomarkers in Alzheimer disease. Nat. Rev. Neurol. 2010; 6:131–144. [PubMed: 20157306]

Busciglio J, Hartmann H, Lorenzo A, Wong C, Baumann K, Sommer B, Staufenbiel M, Yankner BA. Neuronal localization of presenilin-1 and association with amyloid plaques and neurofibrillary tangles in Alzheimer's disease. J. Neurosci. 1997; 17:5101–5107. [PubMed: 9185547]

Buchhave P, Minthon L, Zetterberg H, Wallin AK, Blennow K, Hansson O. Cerebrospinal fluid levels of β-amyloid 1-42, but not of tau, are fully changed already 5 to 10 years before the onset of Alzheimer dementia. Arch. Gen. Psychiatry. 2012; 69:98–106. [PubMed: 22213792]

Cai Y, Xiong K, Zhang XM, Cai H, Luo XG, Feng JC, Clough RW, Struble RG, Patrylo PR, Chu Y, Kordower JH, Yan XX. β-Secretase-1 elevation in aged monkey and Alzheimer's disease human cerebral cortex occurs around the vasculature in partnership with multisystem axon terminal pathogenesis and β-amyloid accumulation. Eur. J. Neurosci. 2010; 32:1223–1238. [PubMed: 20726888]

Cai Y, Zhang XM, Macklin LN, Cai H, Luo XG, Oddo S, Laferla FM, Struble RG, Rose GM, Patrylo PR, Yan XX. BACE1 elevation is involved in amyloid plaque development in the triple transgenic model of Alzheimer's disease: differential Aβ antibody labeling of early-onset axon terminal pathology. Neurotox. Res. 2012; 21:160–174. [PubMed: 21725719]

Chau DM, Crump CJ, Villa JC, Scheinberg DA, Li YM. Familial Alzheimer disease presenilin-1 mutations alter the active site conformation of γ-secretase. J. Biol. Chem. 2012; 287:17288–17296. [PubMed: 22461631]

Chávez-Gutiérrez L, Bammens L, Benilova I, Vandersteen A, Benurwar M, Borgers M, Lismont S, Zhou L, Van Cleynenbreugel S, Esselmann H, Wiltfang J, Serneels L, Karran E, Gijsen H, Schymkowitz J, Rousseau F, Broersen K, De Strooper B. The mechanism of γ-secretase dysfunction in familial Alzheimer disease. EMBO J. 2012; 31:2261–2274. [PubMed: 22505025]

Chui DH, Shirotani K, Tanahashi H, Akiyama H, Ozawa K, Kunishita T, Takahashi K, Makifuchi T, Tabira T. Both N-terminal and C-terminal fragments of presenilin 1 colocalize with neurofibrillary tangles in neurons and dystrophic neurites of senile plaques in Alzheimer's disease. J. Neurosci. Res. 1998; 53:99–106. [PubMed: 9670996]

Cornford EM, Hyman S, Cornford ME, Damian RT. Glut1 glucose transporter in the primate choroid plexus endothelium. J. Neuropathol. Exp. Neurol. 1998; 57:404–414. [PubMed: 9596411]

Dumurgier J, Vercruysse O, Paquet C, Bombois S, Chaulet C, Laplanche JL, Peoc'h K, Schraen S, Pasquier F, Touchon J, Hugon J, Lehmann S, Gabelle A. Intersite variability of CSF Alzheimer's disease biomarkers in clinical setting. Alzheimers Dement. 2012 doi:pii: S1552-5260(12)02381-3.

Engelborghs S, Sleegers K, Cras P, Brouwers N, Serneels S, De Leenheir E, Martin JJ, Vanmechelen E, Van Broeckhoven C, De Deyn PP. No association of CSF biomarkers with APOEepsilon4, plaque and tangle burden in definite Alzheimer's disease. Brain. 2007; 130:2320–2326. [PubMed: 17586559]

Frykman S, Hur JY, Frånberg J, Aoki M, Winblad B, Nahalkova J, Behbahani H, Tjernberg LO. Synaptic and endosomal localization of active gamma-secretase in rat brain. PLoS One. 2010; 5:e8948. [PubMed: 20126630]

Goldstein ME, Cao Y, Fiedler T, Toyn J, Iben L, Barten DM, Pierdomenico M, Corsa J, Prasad CV, Olson RE, Li YW, Zaczek R, Albright CF. Ex vivo occupancy of gamma-secretase inhibitors correlates with brain beta-amyloid peptide reduction in Tg2576 mice. J. Pharmacol. Exp. Ther. 2007; 323:102–108. [PubMed: 17640949]

Hata S, Taniguchi M, Piao Y, Ikeuchi T, Fagan AM, Holtzman DM, Bateman R, Sohrabi HR, Martins RN, Gandy S, Urakami K, Suzuki T. Multiple gamma-secretase product peptides are coordinately increased in concentration in the cerebrospinal fluid of a subpopulation of sporadic Alzheimer's disease subjects. Mol. Neurodegener. 2012; 7:16. [PubMed: 22534039]

Hata S, Fujishige S, Araki Y, Taniguchi M, Urakami K, Peskind E, Akatsu H, Araseki M, Yamamoto K, Martins RN, Maeda M, Nishimura M, Levey A, Chung KA, Montine T, Leverenz J, Fagan A, Goate A, Bateman R, Holtzman DM, Yamamoto T, Nakaya T, Gandy S, Suzuki T. Alternative processing of γ-secretase substrates in common forms of mild cognitive impairment and Alzheimer's disease: evidence for γ-secretase dysfunction. Ann. Neurol. 2011; 69:1026–1031. [PubMed: 21681798]

Hardy J, Allsop D. Amyloid deposition as the central event in the aetiology of Alzheimer's disease. Trends Pharmacol. Sci. 1991; 12:383–388. [PubMed: 1763432]

Holtzman DM. CSF biomarkers for Alzheimer's disease: current utility and potential future use. Neurobiol. Aging. 2011; 32(Suppl 1):S4–9. [PubMed: 22078172]

Huynh DP, Vinters HV, Ho DH, Ho VV, Pulst SM. Neuronal expression and intracellular localization of presenilins in normal and Alzheimer disease brains. J. Neuropathol. Exp. Neurol. 1997; 56:1009–1017. [PubMed: 9291942]

Imbimbo BP, Giardina GA. γ-Secretase inhibitors and modulators for the treatment of Alzheimer's disease: disappointments and hopes. Curr. Top Med. Chem. 2011; 11:1555–1570. [PubMed: 21510832]

Iwatsubo T. The gamma-secretase complex: machinery for intramembrane proteolysis. Curr. Opin. Neurobiol. 2004; 14:379–383. [PubMed: 15194119]

Kaether C, Haass C, Steiner H. Assembly, trafficking and function of gamma-secretase. Neurodegener. Dis. 2006; 3:275–283. [PubMed: 17047368]

Kakuda N, Shoji M, Arai H, Furukawa K, Ikeuchi T, Akazawa K, Takami M, Hatsuta H, Murayama S, Hashimoto Y, Miyajima M, Arai H, Nagashima Y, Yamaguchi H, Kuwano R, Nagaike K, Ihara Y, Japanese Alzheimer's Disease Neuroimaging Initiative. Altered γ-secretase activity in mild cognitive impairment and Alzheimer's disease. EMBO Mol. Med. 2012; 4:344–352. [PubMed: 22354516]

Kalaria RN, Premkumar DR, Pax AB, Cohen DL, Lieberburg I. Production and increased detection of amyloid beta protein and amyloidogenic fragments in brain microvessels, meningeal vessels and choroid plexus in Alzheimer's disease. Brain Res. Mol. Brain Res. 1996; 35:58–68. [PubMed: 8717340]

Kapaki EN, Paraskevas GP, Tzerakis NG, Sfagos C, Seretis A, Kararizou E, Vassilopoulos D. Cerebrospinal fluid tau, phospho-tau181 and beta-amyloid1-42 in idiopathic normal pressure hydrocephalus: a discrimination from Alzheimer's disease. Eur. J. Neurol. 2007; 14:168–173. [PubMed: 17250725]

Kimberly WT, LaVoie MJ, Ostaszewski BL, Ye W, Wolfe MS, Selkoe DJ. Gamma-secretase is a membrane protein complex comprised of presenilin, nicastrin, Aph-1, and Pen-2. Proc. Natl. Acad. Sci. USA. 2003; 100:6382–6387. [PubMed: 12740439]

Koedam EL, van der Vlies AE, van der Flier WM, Verwey NA, Koene T, Scheltens P, Blankenstein MA, Pijnenburg YA. Cognitive correlates of cerebrospinal fluid biomarkers in frontotemporal dementia. Alzheimers Dement. 2012 doi: 10.1016/j.jalz.2011.12.007.

Krut JJ, Zetterberg H, Blennow K, Cinque P, Hagberg L, Price RW, Studahl M, Gisslén M. Cerebrospinal fluid Alzheimer's biomarker profiles in CNS infections. J. Neurol. 2012 doi: 10.1007/s00415-012-6688-y.

Krzyzanowska A, Carro E. Pathological alteration in the choroid plexus of Alzheimer's disease: implication for new therapy approaches. Front. Pharmacol. 2012; 3:75. [PubMed: 22563316]

Laudon H, Mathews PM, Karlstrom H, Bergman A, Farmery MR, Nixon RA, Winblad B, Gandy SE, Lendahl U, Lundkvist J, Naslund J. Co-expressed presenilin 1 NTF and CTF form functional gamma-secretase complexes in cells devoid of full-length protein. J. Neurochem. 2004; 89:44–53. [PubMed: 15030388]

Levey AI, Heilman CJ, Lah JJ, Nash NR, Rees HD, Wakai M, Mirra SS, Rye DB, Nochlin D, Bird TD, Mufson EJ. Presenilin-1 protein expression in familial and sporadic Alzheimer's disease. Ann. Neurol. 1997; 41:742–753. [PubMed: 9189035]

Li YM, Xu M, Lai MT, Huang Q, Castro JL, DiMuzio-Mower J, Harrison T, Lellis C, Nadin A, Neduvelil JG, Register RB, Sardana MK, Shearman MS, Smith AL, Shi XP, Yin KC, Shafer JA, Gardell SJ. Photoactivated gamma-secretase inhibitors directed to the active site covalently label presenilin 1. Nature. 2000; 405:689–694. [PubMed: 10864326]

Lu Y, Riddell D, Hajos-Korcsok E, Bales K, Wood KM, Nolan CE, Robshaw AE, Zhang L, Leung L, Becker SL, Tseng E, Barricklow J, Miller EH, Osgood S, O'Neill BT, Brodney MA, Johnson DS, Pettersson M. Cerebrospinal fluid amyloid-β (Aβ) as an effect biomarker for brain Aβ lowering verified by quantitative preclinical analyses. J. Pharmacol. Exp. Ther. 2012; 342:366–375. [PubMed: 22562771]

Mathews PM, Cataldo AM, Kao BH, Rudnicki AG, Qin X, Yang JL, Jiang Y, Picciano M, Hulette C, Lippa CF, Bird TD, Nochlin D, Walter J, Haass C, Lévesque L, Fraser PE, Andreadis A, Nixon

RA. Brain expression of presenilins in sporadic and early-onset, familial Alzheimer's disease. Mol. Med. 2000; 6:878–891. [PubMed: 11126202]

Mattsson N, Zetterberg H, Hansson O, Andreasen N, Parnetti L, Jonsson M, Herukka SK, van der Flier WM, Blankenstein MA, Ewers M, Rich K, Kaiser E, Verbeek M, Tsolaki M, Mulugeta E, Rosén E, Aarsland D, Visser PJ, Schröder J, Marcusson J, de Leon M, Hampel H, Scheltens P, Pirttilä T, Wallin A, Jönhagen ME, Minthon L, Winblad B, Blennow K. CSF biomarkers and incipient Alzheimer disease in patients with mild cognitive impairment. JAMA. 2009; 302:385–393. [PubMed: 19622817]

Mestres-Ventura P, Morguet A, de las Heras SG. Multi-sensor arrays for online monitoring of cell dynamics in in vitro studies with choroid plexus epithelial cells. Sensors (Basel). 2012; 12:1383–1397. [PubMed: 22438715]

Mollenhauer B, Esselmann H, Trenkwalder C, Schulz-Schaeffer W, Kretzschmar H, Otto M, Wiltfang J, Bibl M. CSF amyloid-β peptides in neuropathologically diagnosed dementia with Lewy bodies and Alzheimer's disease. J. Alzheimers Dis. 2011; 24:383–391. [PubMed: 21297274]

Noguchi M, Yoshita M, Matsumoto Y, Ono K, Iwasa K, Yamada M. Decreased beta-amyloid peptide42 in cerebrospinal fluid of patients with progressive supranuclear palsy and corticobasal degeneration. J. Neurol. Sci. 2005; 237:61–65. [PubMed: 15992827]

Ozudogru SN, Lippa CF. Disease modifying drugs targeting β-amyloid. Am. J. Alzheimers Dis. Other. Demen. 2012; 27:296–300. [PubMed: 22815077]

Otto M, Esselmann H, Schulz-Shaeffer W, Neumann M, Schröter A, Ratzka P, Cepek L, Zerr I, Steinacker P, Windl O, Kornhuber J, Kretzschmar HA, Poser S, Wiltfang J. Decreased beta-amyloid1-42 in cerebrospinal fluid of patients with Creutzfeldt-Jakob disease. Neurology. 2000; 54:1099–1102. [PubMed: 10720281]

Panegyres PK, Toufexis K. Presenilin immunoreactivity in Alzheimer's disease. Eur. J. Neurol. 2005; 12:700–706. [PubMed: 16128871]

Panza F, Frisardi V, Imbimbo BP, Capurso C, Logroscino G, Sancarlo D, Seripa D, Vendemiale G, Pilotto A, Solfrizzi V. REVIEW: γ-Secretase inhibitors for the treatment of Alzheimer's disease: The current state. CNS Neurosci. Ther. 2010; 16:272–284. [PubMed: 20560993]

Parnetti L, Chiasserini D. Role of CSF biomarkers in the diagnosis of prodromal Alzheimer's disease. Biomark. Med. 2011; 5:479–484. [PubMed: 21861669]

Patel S, O'Malley S, Connolly B, Liu W, Hargreaves R, Sur C, Gibson RE. In vitro characterization of a gamma-secretase radiotracer in mammalian brain. J. Neurochem. 2006; 96:171–178. [PubMed: 16300641]

Preston JE. Ageing choroid plexus-cerebrospinal fluid system. Microsc. Res. Tech. 2001; 52:31–37. [PubMed: 11135446]

Pomara N, Bruno D, Sarreal AS, Hernando RT, Nierenberg J, Petkova E, Sidtis JJ, Wisniewski TM, Mehta PD, Pratico D, Zetterberg H, Blennow K. Lower CSF amyloid beta peptides and higher F2-isoprostanes in cognitively intact elderly individuals with major depressive disorder. Am. J. Psychiatry. 2012; 169:523–530. [PubMed: 22764362]

Raemaekers T, Esselens C, Annaert W. Presenilin 1: more than just gamma-secretase. Biochem. Soc. Trans. 2005; 33:559–562. [PubMed: 16042544]

Redzic ZB, Preston JE, Duncan JA, Chodobski A, Szmydynger-Chodobska J. The choroid plexus-cerebrospinal fluid system: from development to aging. Curr. Top. Dev. Biol. 2005; 71:1–52. [PubMed: 16344101]

Rosenmann H. CSF biomarkers for amyloid and tau pathology in Alzheimer's disease. J. Mol. Neurosci. 2012; 47:1–14. [PubMed: 22058061]

Sasaki A, Iijima M, Yokoo H, Shoji M, Nakazato Y. Human choroid plexus is an uniquely involved area of the brain in amyloidosis: a histochemical, immunohistochemical and ultrastructural study. Brain Res. 1997; 55:193–201. [PubMed: 9175887]

Selkoe DJ. Cell biology of the amyloid beta-protein precursor and the mechanism of Alzheimer's disease. Annu. Rev. Cell Biol. 1994; 10:373–403. [PubMed: 7888181]

Serot JM, Bene MC, Foliguet B, Faure GC. Morphological alterations of the choroid plexus in late-onset Alzheimer's disease. Acta Neuropathol. 2000; 99:105–108. [PubMed: 10672315]

Serot JM, Peltier J, Fichten A, Ledeme N, Bourgeois AM, Jouanny P, Toussaint P, Legars D, Godefroy O, Mazière JC. Reduced CSF turnover and decreased ventricular Aβ42 levels are related. BMC Neurosci. 2011; 12:42. [PubMed: 21569454]

Siderowf A, Xie SX, Hurtig H, Weintraub D, Duda J, Chen-Plotkin A, Shaw LM, Van Deerlin V, Trojanowski JQ, Clark C. CSF amyloid 1-42 predicts cognitive decline in Parkinson disease. Neurology. 2010; 75:1055–1061. [PubMed: 20720189]

Silverberg GD, Heit G, Huhn S, Jaffe RA, Chang SD, Bronte-Stewart H, Rubenstein E, Possin K, Saul TA. The cerebrospinal fluid production rate is reduced in dementia of the Alzheimer's type. Neurology. 2001; 57:1763–1766. [PubMed: 11723260]

Skoog I, Davidsson P, Aevarsson O, Vanderstichele H, Vanmechelen E, Blennow K. Cerebrospinal fluid beta-amyloid 42 is reduced before the onset of sporadic dementia: a population-based study in 85-year-olds. Dement. Geriatr. Cogn. Disord. 2003; 15:169–176. [PubMed: 12584433]

Slats D, Claassen JA, Spies PE, Borm G, Besse KT, van Aalst W, Tseng J, Sjögren MJ, Olde Rikkert MG, Verbeek MM. Hourly variability of cerebrospinal fluid biomarkers in Alzheimer's disease subjects and healthy older volunteers. Neurobiol. Aging. 2012; 33:831.e1–9. [PubMed: 21880396]

Spies PE, Verbeek MM, van Groen T, Claassen JA. Reviewing reasons for the decreased CSF Abeta42 concentration in Alzheimer disease. Front. Biosci. 2012; 17:2024–2034. [PubMed: 22652762]

Stern RA, Otvos L Jr, Trojanowski JQ, Lee VM. Monoclonal antibodies to a synthetic peptide homologous with the first 28 amino acids of Alzheimer's disease beta-protein recognize amyloid and diverse glial and neuronal cell types in the central nervous system. Am. J. Pathol. 1989; 134:973–978. [PubMed: 2524164]

Struble RG, Ala T, Patrylo PR, Brewer GJ, Yan XX. Is brain amyloid production a cause or a result of dementia of the Alzheimer's type? J. Alzheimers Dis. 2010; 22:393–399. [PubMed: 20847431]

Thinakaran G, Borchelt DR, Lee MK, Slunt HH, Spitzer L, Kim G, Ratovitsky T, Davenport F, Nordstedt C, Seeger M, Hardy J, Levey AI, Gandy SE, Jenkins NA, Copeland NG, Price DL, Sisodia SS. Endoproteolysis of presenilin 1 and accumulation of processed derivatives in vivo. Neuron. 1996; 17:181–190. [PubMed: 8755489]

Tomidokoro Y, Ishiguro K, Igeta Y, Matsubara E, Kanai M, Shizuka M, Kawarabayashi T, Harigaya Y, Kawakatsu S, Ii K, Ikeda M, St George-Hyslop PH, Hirai S, Okamoto K, Shoji M. Carboxyl-terminal fragments of presenilin-1 are closely related to cytoskeletal abnormalities in Alzheimer's brains. Biochem. Biophys. Res. Commun. 1999; 256:512–518. [PubMed: 10080929]

Vanderstichele H, Bibl M, Engelborghs S, Le Bastard N, Lewczuk P, Molinuevo JL, Parnetti L, Perret-Liaudet A, Shaw LM, Teunissen C, Wouters D, Blennow K. Standardization of preanalytical aspects of cerebrospinal fluid biomarker testing for Alzheimer's disease diagnosis: a consensus paper from the Alzheimer's Biomarkers Standardization Initiative. Alzheimers Dement. 2012; 8:65–73. [PubMed: 22047631]

Vassar R, Kovacs DM, Yan R, Wong PC. The beta-secretase enzyme BACE in health and Alzheimer's disease: regulation, cell biology, function, and therapeutic potential. J. Neurosci. 2009; 29:12787–12794. [PubMed: 19828790]

Weggen S, Diehlmann A, Buslei R, Beyreuther K, Bayer TA. Prominent expression of presenilin-1 in senile plaques and reactive astrocytes in Alzheimer's disease brain. Neuroreport. 1998; 9:3279–3283. [PubMed: 9831464]

Winton MJ, Lee EB, Sun E, Wong MM, Leight S, Zhang B, Trojanowski JQ, Lee VM. Intraneuronal APP, not free Aβ peptides in 3xTg-AD mice: implications for tau versus Aβ-mediated Alzheimer neurodegeneration. J. Neurosci. 2011; 31:7691–7699. [PubMed: 21613482]

Wolburg H, Paulus W. Choroid plexus: biology and pathology. Acta Neuropathol. 2010; 119:75–88. [PubMed: 20033190]

Wolfe MS. γ-Secretase inhibitors and modulators for Alzheimer's disease. J. Neurochem. 2012; 120(Suppl 1):89–98. [PubMed: 22122056]

Xia MQ, Berezovska O, Kim TW, Xia WM, Liao A, Tanzi RE, Selkoe D, Hyman BT. Lack of specific association of presenilin 1 (PS-1) protein with plaques and tangles in Alzheimer's disease. J. Neurol. Sci. 1998; 158:15–23. [PubMed: 9667772]

Xiong K, Clough RW, Luo XG, Struble RG, Li YM, Yan XX. [3H]-L-685,458 as a radiotracer that maps gamma-secretase complex in the rat brain: relevance to Abeta genesis and presence of active presenilin-1 components. Brain Res. 2007a; 1157:81–91. [PubMed: 17512915]

Xiong K, Cai H, Luo XG, Struble RG, Clough RW, Yan XX. Mitochondrial respiratory inhibition and oxidative stress elevate beta-secretase (BACE1) proteins and activity in vivo in the rat retina. Exp. Brain Res. 2007b; 181:435–446. [PubMed: 17429617]

Yan XX, Li T, Rominger CM, Prakash SR, Wong PC, Olson RE, Zaczek R, Li YW. Binding sites of gamma-secretase inhibitors in rodent brain: distribution, postnatal development, and effect of deafferentation. J. Neurosci. 2004; 24:2942–2952. [PubMed: 15044533]

Zhang XM, Cai Y, Xiong K, Cai H, Luo XG, Feng JC, Clough RW, Struble RG, Patrylo PR, Yan XX. Beta-secretase-1 elevation in transgenic mouse models of Alzheimer's disease is associated with synaptic/axonal pathology and amyloidogenesis: implications for neuritic plaque development. Eur. J. Neurosci. 2009; 30:2271–2283. [PubMed: 20092570]

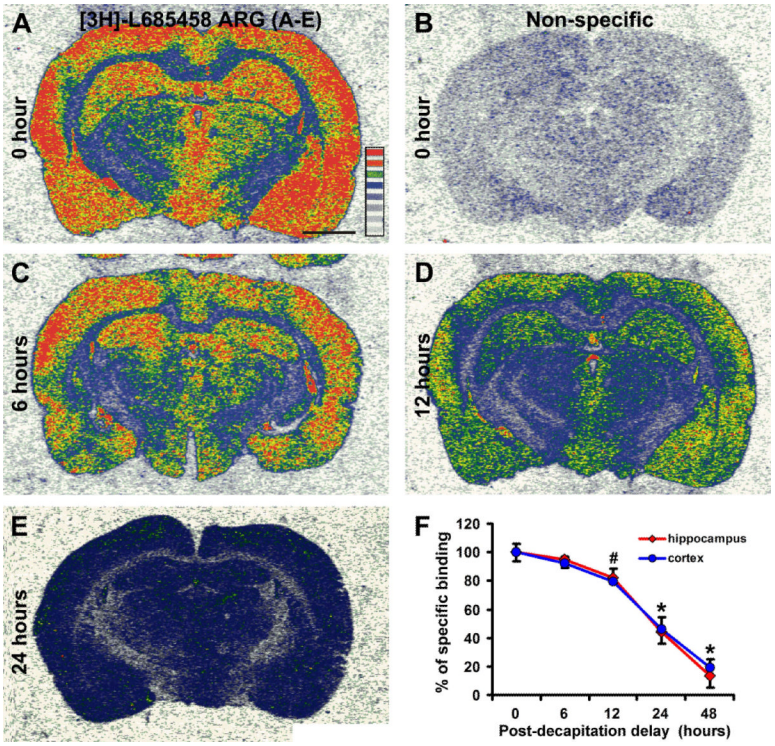

Fig. 1.

Characterization of the effect of delayed brain removal/freezing on [^{3}H]-L-685,458 binding sites in the rat cerebral cortex. Panels (A) and (B) show the total and non-specific radioligand binding in the cortex and hippocampal formation in a fresh frozen brain. Panels (C-E) show reduced radioligand binding density in batch-processed brains removed/frozen 6, 12 and 24 hrs after decapitation. Panel (F) shows a decline in specific binding density (mean ± S.D.) in the parietotemporal cortex and hippocampal formation in the brains collected/frozen 6 to 48 hrs after decapitation, relative to fresh-frozen control (i.e., 0 hr delay, defined as 100%). Scale bar = 200 :m in (A) applying to all image panels.

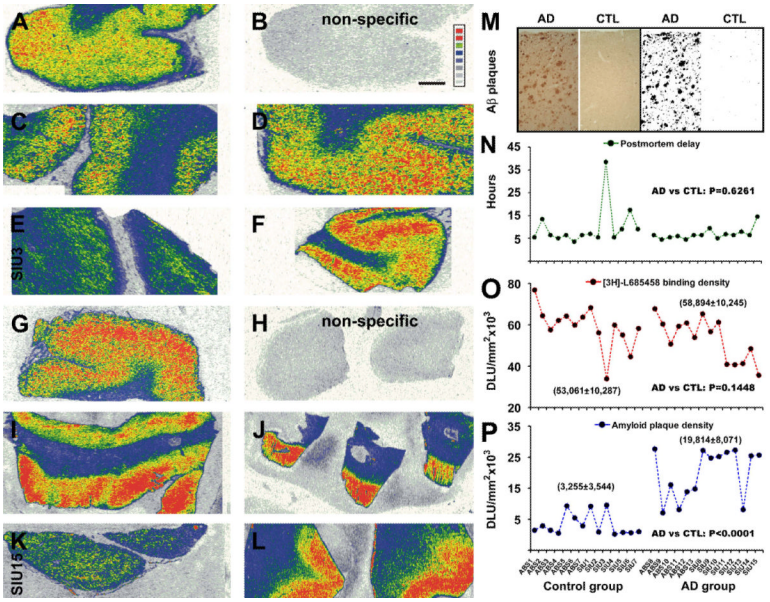

Fig. 2.

Correlative analysis of [^{3}H]-L-685,458 binding sites and amyloid plaques in the temporal neocortex from control and AD subjects. Autoradiographs show cortical γ-secretase binding sites in 5 control (A-F) and 5 AD (G-L) cases. Levels of non-specific binding are shown in (B) and (H). Amyloid plaques are quantified using a threshold selection approach (M). Panel (N) depicts the distribution of postmortem delay among studied cases, with no difference in the means of the control and AD groups. Panel (O) shows the distribution of [^{3}H]-L-685,458 binding sites (averaged from 4 sections) among individual cases, with no difference in the mean specific density between the two groups (58,894±10,245 DLU/mm^2 in AD vs 53,061±10,287 DLU/mm^2 in control). Panel (P) plots the distribution of average amyloid plaque densities among individual cases. The mean density is dramatically higher in the AD (19,814±8,071 DLU/mm^2) than the control (3,255±3,544 DLU/mm^2) group. DLU: digital light unit. Scale bar = 500 :m in (B) applying to all image panels.

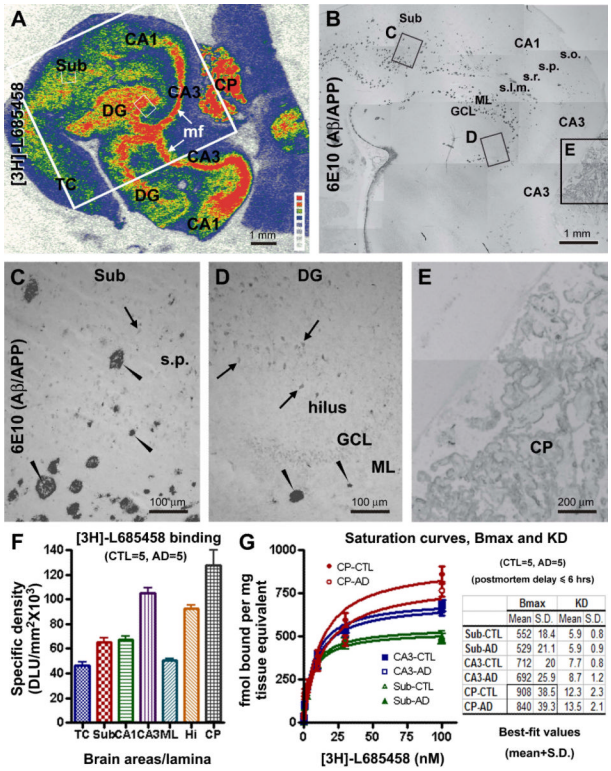

Fig. 3.

Comparative analysis of [^{3}H]-L-685,458 binding sites and amyloid plaques in postmortem human hippocampal formation and choroid plexus (CP). Panel (A) is an autoradiograph of the hippocampal formation from an AD subject. 6E10 immunolabeling, related to extracellular ∃-amyloid (A∃) deposition and potentially intracellular ∃-amyloid precursor protein (APP) expression as well, correspondingly in the large framed area in (A) is shown as panel (B), with 3 boxed areas enlarged as panels (C-E). [^{3}H]-L-685,458 binding sites are mostly dense in the hilus of dente gyrus (DG) and CA3 area corresponding to the mossy fiber (mf) terminal field. The choroid plexus (CP) in the lateral ventricle also exhibits heavy radioligand binding. Moderate binding density occurs in the temporal neocortical (TC) grey matter, the subiculum (Sub), CA1 stratum pyramidale (s.p.) and dentate granule cell layer (GCL). Minimal binding exists in cortical white matter and the hippocampal stratum oriens (s.o.). Amyloid plaques (arrowheads) are mostly located over the molecular layer (ML) of the DG, the strata radiatum (s.r.) and lucunosum-moleculare (s.l.m.) of CA1, and the deep subiculum (B, C, D). Weak 6E10 reactivity is seen in the CP (B, E) and in some pyramidal-like neuronal somata (C, D, arrows). Panel (F) summarizes laminar densitometric data of [^{3}H]-L-685,458 binding sites in temporal lobe structures collectively obtained from 5 control and 5 AD cases with postmortem delays ≤ 6 hrs. Note the higher binding densities in the CP and mossy fiber terminals relative to other lamina. Panel (G) shows that [^{3}H]-L-685,458 binding is saturable in subiculum cortex, CA3 mossy fiber field and the CP (curves derived from one saturation-binding assay). The inserted table summarized the maximal binding density (Bmax) and dissociation constant (KD), for 3 representative regions, the subiculum, CA3 and CP, in the control (n=5) and AD (n=5) groups (with postmortem delay ≤ 6 hrs). The mean of the estimated Bmax in the CP is reduced in the AD relative to the control group (P=0.0456, paired two-tail Student's *t*-test). Scale bars are as indicated in individual image panels.

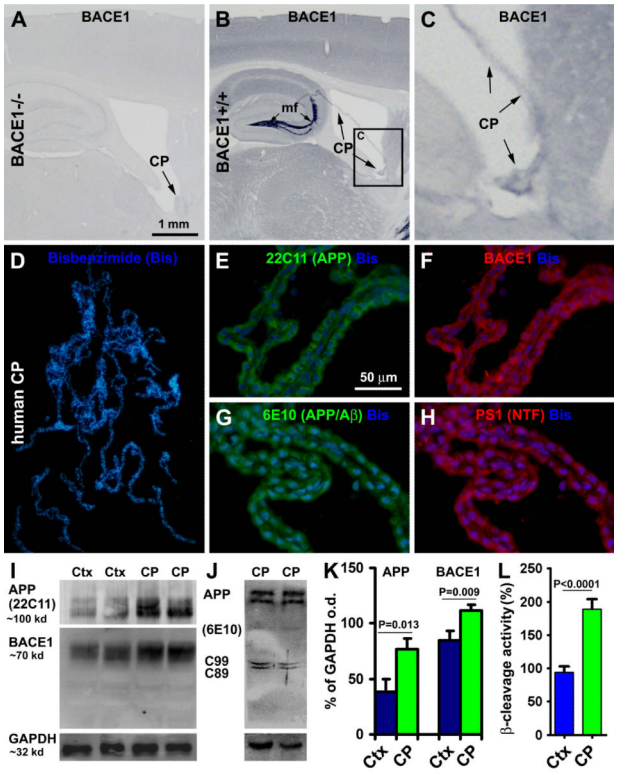

Fig. 4.

Immunohistological and western blot characterization of amyloidogenic proteins and ∃-site cleavage in resected human choroid plexus (CP) and cortical (Ctx) samples (n=5). Panels (A-C) show that BACE1 immunoreactivity (IR) is absent in the CP in BACE1 knockout (BACE1−/−) mouse brain (A), but exists in wild-type (BACE+/+) counterpart (B, C, pointed by arrows). Note the heavy BACE1 IR in the mossy fiber (mf) terminals in (B). Double immunofluorescence with bisbenzimide (Bis) counterstain shows that the CP cells exhibit colocalized IR for ∃-amyloid precusor protein (APP) (22C11 antibody) and BACE1 (D-F), and for 6E10 and presenilin (PS1) (G, H). APP and BACE1 protein levels are higher in human CP than cortical homogenates (I, K). ∃-Site APP cleavage products (C99 and C89) are present in CP extracts (J). ∃-Site APP cleavage activity is higher in the CP relative to cortical extracts (L). Scale bar = 1 mm in (A) applying to (B, D); equal to 200 :m for (C) and 50 :m for (E-H).

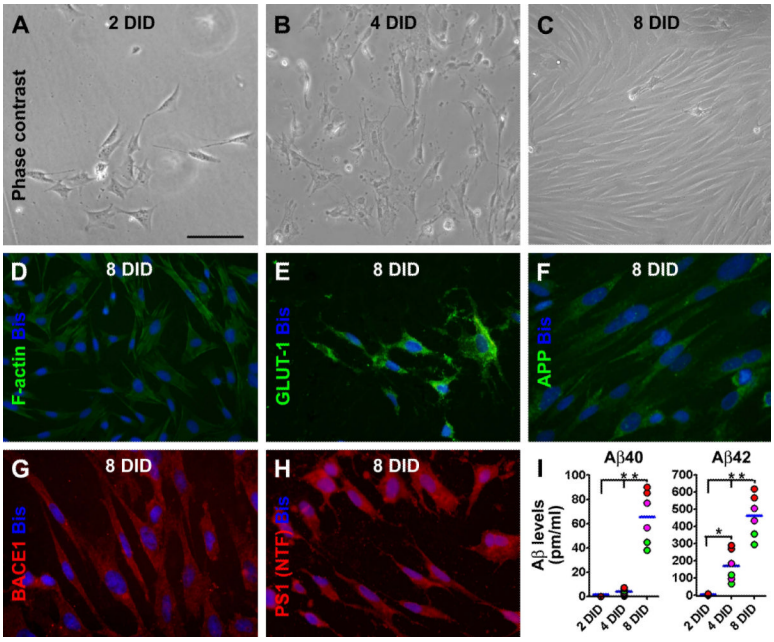

Fig. 5.

Characterization of cultured human choroid plexus cells and their release of AƎ40 and AƎ42. Panels (A-C) show representative phase contrast images of cultured cells at 2 (A), 4 (B) and 8 (C) days in dish (DID). An increase in cell density is noticeable during the examined in vitro period, with the cells appearing mainly polygonal in shape at 2and 4 DID, but mostly fusiform by 8 DID. F-actin immunofluorescence reveals a network of cytoskeleton in individual cells (D). The cultured cells express immunoreactivity for glucose transporter-1 (GLUT-1) (E), Ǝ-amyloid precursor protein (antibody 22C11 labeling) (F), BACE1 (G), and presenilin-1 (PS1) by an antibody (ab14) to the N-terminal fragments (NTF) (H). Bisbenzimide (Bis) nuclear stain is shown in blue (D-H). Levels of AƎ40 and AƎ42 in culture media are minimal at 2DID, and elevate with time in culture, especially for AƎ42 (I). Levels of AƎ42 appear much higher relative to AƎ40 at 4 and 8 DID. The green, purple and red dots in (I) represent means (assayed in duplicate) of medium AƎ concentrations from individual wells of cultured CP cells from the CSU3, 4 and 5 cases listed in Table-1. Scale bar = 100 :m in (A) applying for (B, C), equal to 50 :m for (D-H).

Table-1

Demographic information of human brain samples

Case#	Age	Gender	Clinical diagnosis	Postmortem delay (hrs)
Control group				
ABS1	89	F	liver cancer	5.5
ABS2	71	F	sepsis	13.5
ABS3	73	M	myelodisplastic syndrome	6.5
ABS4	80	M	heart failure	5
ABS5	77	M	colon cancer	6.5
ABS6	89	F	liver cancer	3.5
ABS7	70	M	Sepsis	6.5
SIU1	77	M	colon cancer	7
SIU2	63	M	lung cancer	5.5
SIU3	75	F	ovary cancer	38.5
SIU4	65	F	cardio-respiratory failure	5.5
SIU5	70	F	pneumonia	9
SIU6	73	F	pancreatic cancer	17.5
SIU7	87	M	lung cancer	9
AD group				
ABS8	65	M	heart failure, 3 year dementia	6.5
ABS9	79	F	colon cancer, 5 year dementia	4.5
ABS10	73	M	stroke, 6 year dementia	5.5
ABS11	84	F	end-stage AD	6
ABS12	76	M	end-stage AD	4.5
ABS13	68	M	end-stage AD	6.5
SIU8	81	F	end-stage AD	6.5
SIU9	66	M	end-stage AD	9.5
SIU10	84	M	end-stage AD	5
SIU11	76	M	end-stage AD	6.8
SIU12	83	F	end-stage AD	6.5
SIU13	90	F	AD, heart failure	8
SIU14	73	M	AD/CAA	6.5
SIU15	77	M	AD/CAA	14.6
Biopsy group				
CSU1	49	F	meningiomas	0
CSU2	58	F	astrocytomas	0
CSU3	62	M	astrocytomas	0
CSU4	53	F	astrocytomas	0
CSU5	57	F	choroid plexus papilloma	0